Proceedings of the Sixteenth International Conference on
Computational Structures Technology
Edited by: P. Iványi, J. Kruis and B.H.V. Topping
Civil-Comp Conferences, Volume 14, Paper 15.2
Civil-Comp Press, Edinburgh, United Kingdom, 2026
ISSN: 2753-3239, doi: 10.4203/ccc.14.15.2

Improved DKMT18 and DKMQ24 Shell Elements With Pseudo-Curvatures

R. S. Katili[1], I. Katili[1], S. Natarajan[2] and S. P. A. Bordas[3,4]

[1]Department of Civil Engineering, University of Indonesia, Depok, Indonesia
[2]Department of Mechanical Engineering, Indian Institute of Technology Madras, Chennai, India
[3]Faculté des Sciences, de la Technologie et de la Communication, University of Luxembourg, Luxembourg
[4]Department of Engineering, University of Exeter, United Kingdom

Abstract

This paper presents the improvement of the 3-node triangular DKMT18 (2020) and 4-node quadrilateral DKMQ24 (2015) curved shell element by applying pseudo-normal vectors to the corner vertices, which are then used to obtain the pseudo-curvatures. The improved DKMT18 and DKMQ24 curved shell element represents full coupling of membrane-bending in bending strains. The assumed transverse shear strains are used to avoid shear locking. Both elements pass the patch tests, are locking-free, have a proper rank, perform well, provide convergent results, and show significant improvement in the twisted beam and Raasch's hook problem compared to the previous version.

Keywords: shell, Reissner-Mindlin-Naghdi shell model, triangular and quadrilateral curved shell elements, 3-node and 4-node finite elements, shear locking free, mixed transverse shear strains, pseudo-curvatures

1 Introduction

In structural mechanics, the efficient calculation of thin to moderately thick shell structures using the finite element method requires reliable and robust elements. These elements must yield precise solutions for arbitrary shell geometries, consider membrane effects, coupled membrane-bending for curvatures, and transverse shear effects.

The Reissner-Naghdi shell theory [1-2] incorporates transverse shear strains and applies from thin to moderately thick shells. This model separates strains into in-plane and out-of-plane components, with bending strains expressed as first derivatives of the displacement, thereby requiring only C^0 continuity. However, shell elements that consider transverse shear strains may experience shear locking in thin shells. To overcome shear locking, the ANS (assumed natural strain) field is applied to out-of-plane components, in this case, the transverse shear strains. The ANS approach is adopted in the formulation of DKMT18 [3] and DKMQ24 [4] shell elements. The two elements perform well in standard benchmark tests except in twisted beam (DKMT18 [3]) and Raasch's hook problems (DKMT18 [3] and DKMQ24 [4]), in which the results deviate from the reference.

The primary objective of this study is to improve the triangular DKMT18 [3] and quadrilateral DKMQ24 [4] shell elements by incorporating pseudo-curvatures to resolve Raasch's hook problem. The new DKMT18 and DKMQ24 shell element features three displacements and three rotational degrees of freedom.

2 Formulation of the improved DKMT18 and DKMQ24 elements

2.1 Geometric description

Figure 1 illustrates the quadrilateral shell element in global coordinates. The geometric function of the mid-surface ($z = 0$) is:

$$\mathbf{x} = X\ \mathbf{i} + Y\ \mathbf{j} + Z\ \mathbf{k}$$
$$X = \sum_{i}^{n_i} N_i X_i\ ;\ Y = \sum_{i}^{n_i} N_i\ Y_i\ ;\ Z = \sum_{i}^{n_i} N_i\ Z_i \tag{1}$$

X, Y, and Z are expressed in curvilinear parametric coordinates (ξ, η). X_i, Y_i, Z_i are the nodal coordinates at node i, N_i are the linear shape functions, and n_i is the number of corner nodes. The covariant vectors $\mathbf{a}_1$ and $\mathbf{a}_2$ in Figure 1 are given by:

$$\mathbf{a}_1 = \frac{\partial \mathbf{x}}{\partial \xi} = \mathbf{x},_{\xi}\ ;\ \mathbf{a}_2 = \frac{\partial \mathbf{x}}{\partial \eta} = \mathbf{x},_{\eta} \tag{2}$$

$\mathbf{a}_1$ and $\mathbf{a}_1$ are covariant vectors that, in general, are not mutually orthogonal.

The unit vectors $\mathbf{t}_1, \mathbf{t}_2, \mathbf{n}$ of the local systems x, y, z are derived from:

$$\begin{aligned}
&\mathbf{n} = \frac{\mathbf{a}_1 \times \mathbf{a}_2}{\|\mathbf{a}_1 \times \mathbf{a}_2\|} \\
&\mathbf{t}_1 = \frac{\mathbf{k} \times \mathbf{n}}{\|\mathbf{k} \times \mathbf{n}\|} \\
&\mathbf{t}_2 = \mathbf{n} \times \mathbf{t}_1 \\
&\text{if } \mathbf{n} = \pm\,\mathbf{k} \text{ then } \mathbf{t}_1 = \pm\,\mathbf{i}
\end{aligned} \tag{3}$$

The derivatives of the functions x and y, with respect to ξ and η, are as follows:

$$\begin{Bmatrix} dx \\ dy \end{Bmatrix} = \begin{bmatrix} t_1.\mathbf{a}_1 & t_1.\mathbf{a}_2 \\ t_2.\mathbf{a}_1 & t_2.\mathbf{a}_2 \end{bmatrix} \begin{Bmatrix} d\xi \\ d\eta \end{Bmatrix} \tag{4}$$

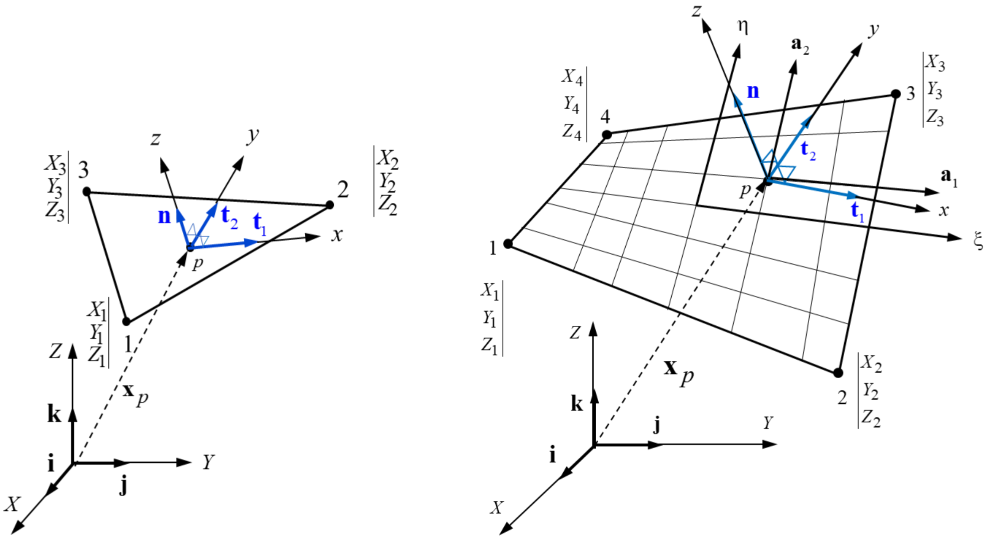

Figure 1: Geometry of triangular and quadrilateral Shell Element.

The inverse of Equation (4) can be expressed as:

$$\begin{Bmatrix} d\xi \\ d\eta \end{Bmatrix} = \begin{bmatrix} j_{11} & j_{12} \\ j_{21} & j_{22} \end{bmatrix}^T \begin{Bmatrix} dx \\ dy \end{Bmatrix}$$
$$\begin{bmatrix} j_{11} & j_{12} \\ j_{21} & j_{22} \end{bmatrix} = \begin{bmatrix} \mathbf{t}_1 . \mathbf{a}_1 & \mathbf{t}_1 . \mathbf{a}_2 \\ \mathbf{t}_2 . \mathbf{a}_1 & \mathbf{t}_2 . \mathbf{a}_2 \end{bmatrix}^{-T} \quad (5)$$

j_{11}, j_{12}, j_{21}, and j_{22} are the terms of the Jacobian inverse.
The dA element is:

$$dA = \left\| \mathbf{a}_1 \times \mathbf{a}_2 \right\| d\xi d\eta \quad (6)$$

Using the Jacobian inverse, the derivatives of shape functions N_i and P_k with respect to x and y:

$$N_{i,x} = N_{i,\xi} j_{11} + N_{i,\eta} j_{12} \; ; N_{i,y} = N_{i,\xi} j_{21} + N_{i,\eta} j_{22}$$
$$P_{k,x} = P_{k,\xi} j_{11} + P_{k,\eta} j_{12} \; ; P_{k,y} = P_{k,\xi} j_{21} + P_{k,\eta} j_{22} \quad (7)$$

2.2 Displacement functions and pseudo-normal vector

The DKMT18 and DKMQ24 shell elements have three translations and three rotations along the unit vector $\mathbf{i}, \mathbf{j}, \mathbf{k}$, as seen in Figure 2.

The displacement vector at $z = 0$:

$$\mathbf{u} = \sum_{i=1}^{n_i} N_i(\xi, \eta) \begin{Bmatrix} U_i \\ V_i \\ W_i \end{Bmatrix} \quad (8)$$

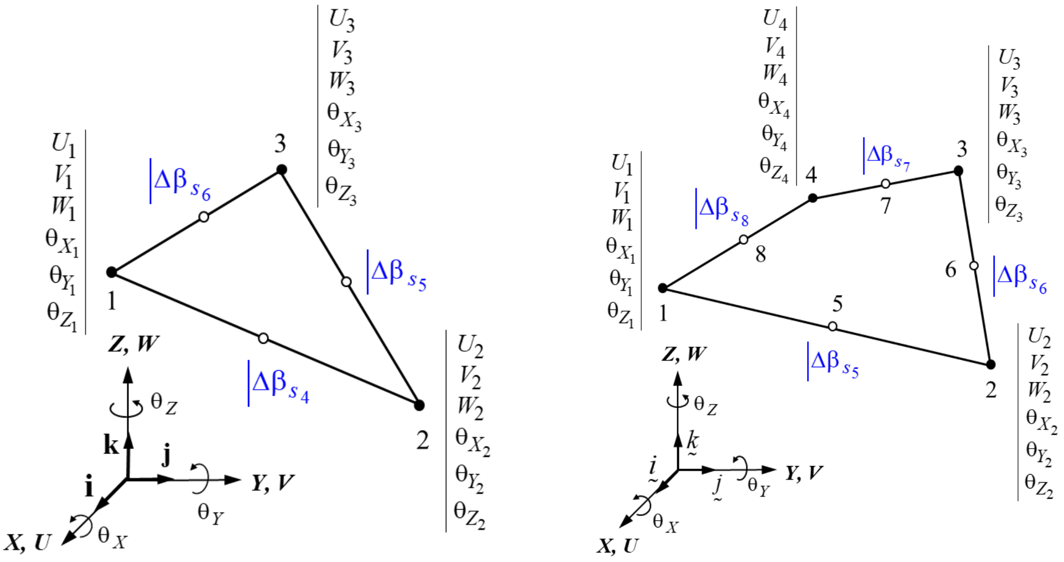

Figure 2: Six DOFs at the corner node and provisional DOF at the mid-side node.

In Figure 3, a pseudo-normal vector $\hat{\mathbf{n}}_i$ is shown. The new formulation of DKMT18 and DKMQ24 uses a pseudo-normal vector $\hat{\mathbf{n}}_i = \left\langle \hat{n}_{X_i} \;\; \hat{n}_{Y_i} \;\; \hat{n}_{Z_i} \right\rangle$ at each corner node i to ensure the continuity of the normal vector across the adjacent elements.

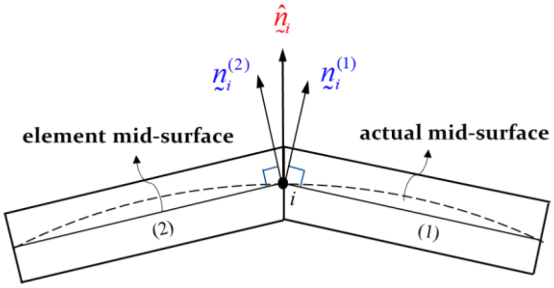

Figure 3: Pseudo-normal vector $\hat{\mathbf{n}}_i$ and the normal vector of the elements $\mathbf{n}_i^{(1)}, \mathbf{n}_i^{(2)}$.

For the improved DKMT18 and DKMQ24, the rotation is represented using pseudo-normal, as follows:

$$\hat{\boldsymbol{\beta}} = \sum_i^{n_i} N_i(\xi,\eta)\left[R\hat{n}_i\right]\begin{Bmatrix}\theta_{Xi}\\ \theta_{Yi}\\ \theta_{Zi}\end{Bmatrix} + \sum_k^{n_k} P_k(\xi,\eta)\,\mathbf{t}_{s_k}\Delta\beta_{s_k} \;\;;\;\; \mathbf{t}_{s_k} = \frac{\mathbf{x}_{ji}}{L_k}$$

$$\left[R\hat{n}_i\right] = \left\langle \mathbf{R\hat{n}}1_i \quad \mathbf{R\hat{n}}2_i \quad \mathbf{R\hat{n}}3_i \right\rangle = \begin{bmatrix} 0 & \hat{n}_{Z_i} & -\hat{n}_{Y_i} \\ -\hat{n}_{Z_i} & 0 & \hat{n}_{X_i} \\ \hat{n}_{Y_i} & -\hat{n}_{X_i} & 0 \end{bmatrix} \tag{9}$$

L_k denotes the length of side k. $\Delta\beta_{s_k}$ are the temporary DOFs at node k shown in Figure 2, and P_k are the quadratic shape functions.

2.3 Membrane, pseudo-curvatures, and transverse shear strains

The membrane strains are:

$$\{e\}=\begin{Bmatrix} e_x \\ e_y \\ e_{xy} \end{Bmatrix}=\begin{Bmatrix} \mathbf{t}_1 \cdot \mathbf{u},_x \\ \mathbf{t}_2 \cdot \mathbf{u},_y \\ \mathbf{t}_1 \cdot \mathbf{u},_y + \mathbf{t}_2 \cdot \mathbf{u},_x \end{Bmatrix} \tag{10}$$

$\mathbf{t}_1$ and $\mathbf{t}_2$ at an arbitrary point p shown in Figure 1 are given in (3). Substituting Equation (8) into Equation (10) gives the membrane strain matrix $[B_m]$ as:

$$\begin{aligned} &\{e\}=[B_m]\{u_n\} \\ &\langle u_n \rangle = \langle \dots\ U_i\ V_i\ W_i\ \theta_{X_i}\ \theta_{Y_i}\ \theta_{Z_i}\ \cdots \rangle \end{aligned} \tag{11}$$

The pseudo-curvatures of the improved DKMT18 and DKMQ24 elements are:

$$\begin{aligned} &\{\chi\}=\begin{Bmatrix} \chi_x \\ \chi_y \\ \chi_{xy} \end{Bmatrix}=\begin{Bmatrix} \mathbf{t}_2 \cdot \hat{\mathbf{n}},_x \\ -\mathbf{t}_1 \cdot \hat{\mathbf{n}},_y \\ \mathbf{t}_2 \cdot \hat{\mathbf{n}},_y - \mathbf{t}_1 \cdot \hat{\mathbf{n}},_x \end{Bmatrix}\Omega+\begin{Bmatrix} \mathbf{t}_1 \cdot \boldsymbol{\beta},_x \\ \mathbf{t}_2 \cdot \boldsymbol{\beta},_y \\ \mathbf{t}_1 \cdot \boldsymbol{\beta},_y + \mathbf{t}_2 \cdot \boldsymbol{\beta},_x \end{Bmatrix} \\ &\Omega=\frac{1}{2}\left(\mathbf{t}_2 \cdot \mathbf{u},_x - \mathbf{t}_1 \cdot \mathbf{u},_y\right) \end{aligned} \tag{12}$$

Substituting Equations (8) and (9) into Equation (12) results in the in-plane bending strains for the improved DKMT18 and DKMQ24 as follows:

$$\{\chi\}=\left[B_{b_u}\right]\{u_n\}+\left[B_{b_\Delta}(\xi,\eta)\right]\left\{\Delta\beta_{s_n}\right\} \tag{13}$$

$$\text{DKMT18}: \left\langle \Delta\beta_{s_n} \right\rangle = \left\langle \Delta\beta_{s_4}\ \Delta\beta_{s_5}\ \Delta\beta_{s_6} \right\rangle$$

$$\text{DKMQ24}: \left\langle \Delta\beta_{s_n} \right\rangle = \left\langle \Delta\beta_{s_5}\ \Delta\beta_{s_6}\ \Delta\beta_{s_7}\ \Delta\beta_{s_8} \right\rangle$$

The kinematic transverse shear strain γ_{s_k} in the s-direction is defined by:

$$\gamma_{s_k} = \hat{\mathbf{n}} \cdot \mathbf{u},_s + \mathbf{t}_{s_k} \cdot \hat{\boldsymbol{\beta}} \tag{14}$$

Constant kinematic transverse shear strains $\underline{\gamma}_{s_k}$, as shown in Figure 4, can be obtained as follows:

$$\underline{\gamma}_{s_k} = \frac{1}{L_k}\int_0^{L_k} \gamma_{s_k}\, ds \quad ; \quad k=5,6,7,8 \tag{15}$$

Substituting Equation (14) into Equation (15) and applying it to all sides, we obtain:

$$\left\{\underline{\gamma}_{s_n}\right\} = \left[A_u\right]\left\{u_n\right\} + \left[A_\Delta\right]\left\{\Delta\beta_{s_n}\right\} \tag{16}$$

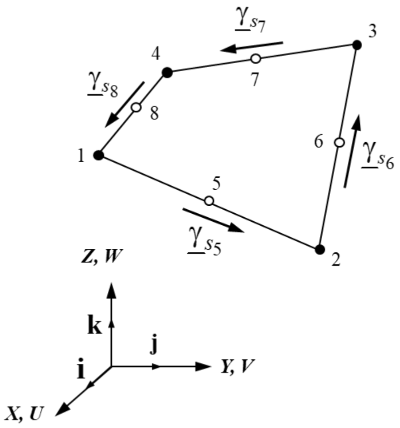

Figure 4: Constant $\underline{\gamma}_{s_k}$ on side *i-j*.

The mixed transverse shear strain $\underline{\gamma}_{s_k}$ alongside k [3, 4] can be expressed as:

$$\underline{\gamma}_{s_k} = \frac{D_b}{D_s}\beta_{s,ss} = -\frac{2}{3}\phi_k\Delta\beta_{s_k} \;\; ; \;\; \phi_k = \frac{D_b}{D_s}\frac{12}{L_k^2} = \frac{2}{\kappa(1-\upsilon)}\left(\frac{h^2}{L_k^2}\right) \tag{17}$$

The factor ϕ_k is a measure of the effect of transverse shear strains on a plate or shell structure. In thin-shell cases, the factor $\phi_k \approx 0$, the transverse shear strains are naturally diminished. This method immediately resolves shear locking, making it its primary benefit. Imposing Equation (17) on the four sides, the following expression is obtained:

$$\left\{\underline{\gamma}_{s_n}\right\} = \left[A_\phi\right]\left\{\Delta\beta_{s_n}\right\} \tag{18}$$

By equating Equation (16) and Equation (18), we obtain:

$$\left[A_u\right]\left\{u_n\right\} + \left[A_\Delta\right]\left\{\Delta\beta_{s_n}\right\} = \left[A_\phi\right]\left\{\Delta\beta_{s_n}\right\} \tag{19}$$

From Equation (19), the $\left\{\Delta\beta_{s_n}\right\}$ can be obtained as follows:

$$\left\{\Delta\beta_{s_n}\right\} = \left[A_n\right]\left\{u_n\right\} \tag{20}$$

To avoid the shear locking, special treatment with ANS (assumed natural strain) is used as follows [3, 4]:

$$\left\{\underline{\gamma}\right\} = \begin{Bmatrix} \underline{\gamma}_x \\ \underline{\gamma}_y \end{Bmatrix} = \left[B_{s_\gamma}\right]\left\{\underline{\gamma}_{s_n}\right\} \tag{21}$$

Introducing Equation (18) and Equation (20) into Equation (21), we get:

$$\{\underline{\gamma}\} = [B_s]\{u_n\} \tag{22}$$

2.4 Membrane, bending, and transverse shear stiffness

The membrane stiffness for the DKMT18 and DKMQ24 elements is:

$$[k_m] = \int_A [B_m]^T [H_m][B_m] dA$$

$$[H_m] = \frac{Eh}{\left(1-\upsilon^2\right)} \begin{bmatrix} 1 & \upsilon & 0 \\ \upsilon & 1 & 0 \\ 0 & 0 & \dfrac{(1-\upsilon)}{2} \end{bmatrix} \tag{23}$$

Substituting Equation (20) into Equation (13), we get the final bending strains:

$$\{\chi\} = [B_b]\{u_n\} \; ; \; [B_b] = \left[B_{b_u}\right] + \left[B_{b_\Delta}\right][A_n] \tag{25}$$

The bending stiffness is:

$$[k_b] = \int_A [B_b]^T [H_b][B_b] dA$$

$$[H_b] = \frac{Eh^3}{12\left(1-\upsilon^2\right)} \begin{bmatrix} 1 & \upsilon & 0 \\ \upsilon & 1 & 0 \\ 0 & 0 & (1-\upsilon)/2 \end{bmatrix} \tag{26}$$

The transverse shear stiffness:

$$[k_s] = \int_A [B_s]^T [H_s][B_s] dA$$

$$[H_s] = \kappa G h \begin{bmatrix} 1 & 0 \\ 0 & 1 \end{bmatrix} \; ; \; \kappa = 5/6 \; ; \; G = \frac{E}{2(1+\upsilon)} \tag{27}$$

2.5 Artificial rotational stiffness and total stiffness

To avoid the singularity problem, we introduce an artificial rotational stiffness related to the variable θ_{z_i} :

$$\left[k_{\theta_z}\right] = 10^{-6} \times D_b \times \frac{h}{\sqrt{A}} \int_A \left\{B_{\theta_z}\right\}\left\langle B_{\theta_z}\right\rangle dA \tag{28}$$

$$\left\langle B_{\theta_z}\right\rangle = \left\langle \cdots \; 0 \; 0 \; 0 \; \hat{n}_{X_i} N_i \; \hat{n}_{Y_i} N_i \; \hat{n}_{Z_i} N_i \; \ldots \; i \; = 1,4 \right\rangle \tag{29}$$

The fictitious stiffness with a rank of 4 eliminates the singularity when the elements are coplanar. The stiffness matrix for DKMT18 and DKMQ24 is:

$$[k] = [k_m] + [k_b] + [k_s] + \left[k_{\theta_z}\right] \tag{30}$$

3 Numerical results

3.1 Twisted beam

The twisted beam problem, introduced by MacNeal and Harder [5], is modelled as a helicoidal shell clamped at one end and twisted by 90° from point O to point A, as illustrated in Figure 5. The modulus of elasticity $E = 29 \times 10^6$; Poisson's ratio = 0.22. Concentrated loads are applied at point A (the free tip centre) in two cases: the first with $P_X = 1000$ and $P_Z = 0$; and the second with $P_X = 0$ and $P_Z = 1000$. The geometry at mid surface is given by: $X = s \cos\theta$; $Y = 2\,\theta\,L/\pi$, $Z = s \sin\theta$ ($-0.5b \leq s \leq +0.5b$ and $0 \leq \theta \leq \pi/2$). The structure is analysed using $N\times6N\times2$ meshes, with N number of elements along the width.

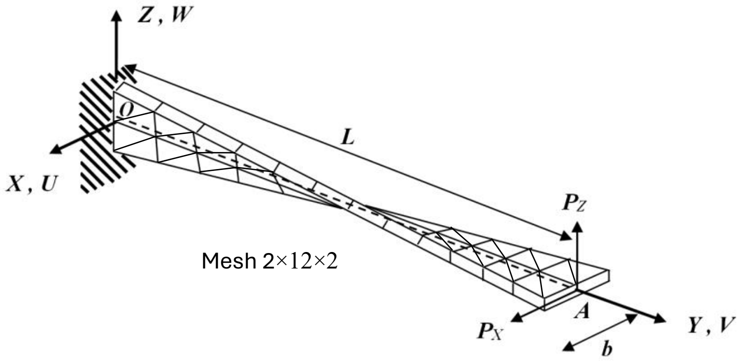

Figure 5: Twisted beam with $N = 2$ mesh (L = 12; b = 1.1; h = 0.32).

The corresponding values at point A are taken from reference [5]: $U_{ref} = 5.424$ and $W_{ref} = 1.754$. The numerical results are presented in Tables 1 and 2.

N	**DKMT18 [3]**	**DKMT18**	**DKMQ24 [4]**	**DKMQ24**
2	5.408	5.318	5.396	5.396
4	6.084	5.372	5.406	5.406
8	9.953	5.401	5.413	5.413
16	25.096	5.412	5.415	5.415
32	71.614	5.415	5.416	5.416
Ref. MacNeal and Harder [6]: $U_{ref} = 5.424$				

Table 1: U_A results for twisted beam $P_X = 1000$ and $P_Z = 0$.

N	**DKMT18 [3]**	**DKMT18**	**DKMQ24 [4]**	**DKMQ24**
2	1.488	1.461	1.625	1.625
4	1.814	1.621	1.713	1.713
8	2.953	1.711	1.742	1.742
16	7.522	1.742	1.750	1.750
32	24.395	1.750	1.752	1.752
Ref. MacNeal and Harder [5]: $W_{ref} = 1.754$				

Table 2: W_A results for twisted beam under $P_X = 0$ and $P_Z = 1000$.

The DKMT18 [3] element exhibits divergent behaviour. This contrasts with the improved DKMT18, which produces accurate results despite also considering shear strains. The authors believe that the good performance is due to the full coupling of membrane bending in the curvatures considered in DKMT18 with pseudo-curvatures. The DKMQ24 [4] and improved DKMQ24 elements yield excellent results that converge towards the reference solutions.

3.2 The Raasch's hook

The Raasch's hook structure [6], with the geometrical structure shown in Figure 6, is also considered to assess the stability of the improved DKMT18 and DKMQ24 elements. It is a complex case for a shell element, given the intrinsic interaction among the three deformation modes (bending, extension, and twist). Many shell elements fail this evaluation and demonstrate divergence in tip displacement, including the previous version of DKMT18 [3] and DKMQ24 [4]. The Raasch's hook problem consists of two joined strips of circular arcs entirely clamped at B and subjected to a load $P = 1.0$ at point A applied in the width direction.

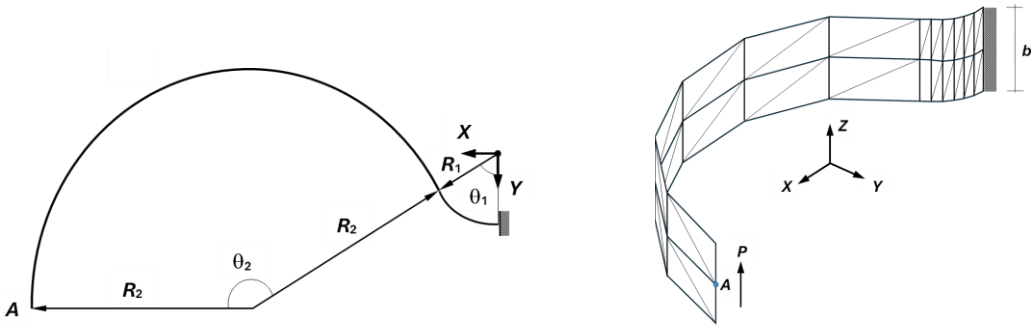

Figure 6: Raasch's Hook problem with 2×12 mesh ($b = 20$, $h = 2$)

Table 3 summarises the vertical displacements at point A on the free edge obtained using $N\times6N$ meshes, $3N$ elements for the $R_1 = 14$, $\theta_1 = 60^o$ and $3N$ elements for the $R_2 = 46$, $\theta_1 = 150^o$. The modulus of elasticity $E = 3.3\times10^3$ and Poisson ratio $\upsilon = 0.3$. The reference displacement at point A: $W_A = 4.825$ for $\upsilon = 0.3$, is obtained from Ko et al. [7].

$N\times6N$	DKMT18 [3]	DKMT18	DKMQ24 [4]	DKMQ24
2×12	4.285	4.450	4.411	4.549
4×24	4.621	4.551	5.025	4.583
8×48	5.312	4.620	6.332	4.654
16×96	7.363	4.719	9.190	4.769
32×192	13.506	4.807	18.347	4.833
Ref. Ko et al. [7] : $W_A = 4.825$				

Table 3: Displacement W_A for Raasch's hook with $\upsilon = 0.3$.

The differences between the improved DKMT18 element results and the reference values are 0.37% ($N = 32$) for $\upsilon = 0.30$. The improved DKMQ24 element closely matches the reference solution, with only 0.17% difference at $N = 32$. Conversely, the DKMT18 [3] and DKMQ24 [4] elements exhibit results that deviated from the reference value.

4 Conclusions and Contributions

A refinement of the previously developed DKMT18 [3] and DKMQ24 [4] has been proposed based on the Reissner-Naghdi shell model. The improved DKMT18 and DKMQ24 elements introduce node-wise pseudo-normal vectors to ensure normal continuity and pseudo-curvatures to compute bending energy more accurately.

A key outcome is the stable performance of the improved DKMT18 and DKMQ24 on the twisted beam and Raasch's hook problems, on the Raasch's hook problem.

Acknowledgements

The authors gratefully acknowledge financial support from the Indonesian Endowment Fund for Education (LPDP) on behalf of the Indonesian Ministry of Higher Education, Science and Technology, administered through the EQUITY Program (Contract No. 4302/B3/DT.03.08/ 2025 and 573/PKS/R/UI/2025).

References

[1] E. Reissner, "The Effect of Transverse Shear Deformation on the Bending of Elastic Plates", Journal of Applied Mechanics in Engineering ASME 1945, 12, A69-A77.

[2] P.M. Naghdi, "On the Theory of Thin Elastic Shells", Quarterly of Applied Mathematics, 14, 369-380, 1957.

[3] I.J. Maknun, I. Katili, A. Ibrahimbegović, J.L. Batoz, "A New Triangular Shell Element for Composites Accounting for Shear Deformation", Composite Structures, 243, 112214, 2020, DOI:10.1016/j.compstruct.2020.112214.

[4] I. Katili, J.L. Batoz, I.J. Maknun, A. Hamdouni, O. Millet, "The Development of DKMQ Plate Bending Element for Thick to Thin Shell Analysis based on the Naghdi/Reissner/Mindlin Shell Theory", Finite Elements in Analysis and Design, 100, 12–27, 2015, DOI:10.1016/j.finel.2015.02.005.

[5] R.H. MacNeal, R.L. Harder, "A Proposed Standard Set of Problems to Test Finite Element Accuracy", Finite Elements in Analysis and Design, 1, 3-20, 1985, DOI:10.1016/0168-874X(85)90003-4.

[6] N.F. Knight Jr., "Raasch Challenge for Shell Elements", AIAA Journal, 35, 375–81, 1997, DOI:10.2514/2.104.

[7] Y. Ko, Y. Lee, P.S. Lee, K.J. Bathe, "Performance of the MITC3+ and MITC4+ shell elements in widely used benchmark problems", Computers and Structures, 193, 187–206, 2017, DOI:10.1016/j.compstruc.2017.08.003.